Crystal structure prediction and simulations of structural transformations: metadynamics and evolutionary algorithms

R. MARTOŇÁK*†, A. R. OGANOV‡§ and C. W. GLASS‡

†Faculty of Mathematics, Physics and Informatics,
Department of Experimental Physics, Comenius University,
Mlynská dolina F2, 842 48 Bratislava, Slovakia
‡Laboratory of Crystallography, Department of Materials ETH Zurich,
HCI G 515, Wolfgang-Pauli-Str. 10, CH-8093 Zurich, Switzerland
§Geology Department, Moscow State University, 119992 Moscow, Russia

Crystal structure prediction is the central problem of computational crystallography and materials design. We review two recently proposed methodologies that address this problem: (1) metadynamics-based approach proposed by R. Martoňák, A. Laio and M. Parrinello, Phys. Rev. Lett. **90** 075503 (2003) and (2) *ab initio* evolutionary algorithm USPEX developed by Glass and Oganov in 2004–2006. The two methods are largely complementary. Metadynamics enables studies of phase transformation mechanisms and can predict new crystal structures, but such simulations require a reasonable starting structure and rely on the choice of a relevant order parameter. Evolutionary simulations cannot find phase transformation mechanisms, but can very efficiently find the stable structure without any knowledge of possible crystal structure or order parameters driving phase transitions. We review several cases where these methods produced important new results: prediction of new phases of $MgSiO_3$ in the Earth's lower mantle, elucidation of plastic behaviour of $MgSiO_3$ phases in the Earth's D'' layer, phase transformation mechanisms of SiO_2 polymorphs, prediction of new high-pressure phases of $CaCO_3$, elemental sulphur and carbon. Further developments of the two methods are outlined.

Keywords: Structural transitions; Crystal structure prediction; Computer simulations; Metadynamics

1. Introduction

Crystal structure prediction is one of the central problems in modern science. While there are different formulations of the problem, our formulation is "to find the stable crystal structure of a given compound at given P–T conditions, knowing only the chemical formula". Solving this problem would allow one to explore matter at conditions unattainable in experiment (e.g., in interiors of giant planets), design new materials by computation, and solve structures that pose problems to experiment

---

*Corresponding author. Email: martonak@fmph.uniba.sk

(difficult structures with insufficient quality of the sample, especially in high-pressure experiments). It was noted almost 20 years ago by Maddox (1988) that the failure to solve this problem is "one of the continuing scandals in the physical sciences". A decade later and in spite of several developments such as simulated annealing [1, 2] and a fixed-cell genetic algorithm [3], Ball (Ref. [4]) wrote that "in large part the scandal remains".

The main difficulty in crystal structure prediction stems from the multidimensionality of the free energy surface and the presence of an enormous number of local minima separated by energy barriers. The (often high) barriers invalidate molecular dynamics (MD) and Monte Carlo (MC) methods as tools for crystal structure prediction, whereas the overwhelming number of local minima makes exhaustive search impossible. One can estimate the number of distinct structures [5] and see its factorial increase with the system size – for an element A (compound AB) it is 10^{11} (10^{14}) for a system with only 10 atoms in the unit cell, 10^{25} (10^{30}) for a system with 20 atoms in the cell, and 10^{39} (10^{47}) for the case of 30 atoms in the unit cell. To cope with these overwhelming numbers, two lines of thought have been employed: (1) semilocal methods, usually starting from some low-energy structure (so that minimum effort is wasted on sampling poor regions of the energy surface) and exploring the neighbourhood of this and subsequently found structures, and (2) global methods, usually starting with randomly generated structures and iteratively "zooming in" on the most promising areas of the free energy surface until the best structure is found. Metadynamics [6–8], simulated annealing [1, 2], basin hopping [9] and minima hopping [10] approaches belong to the first category, while the second category is represented by evolutionary algorithms [3, 5, 11–13]. Different methods can often be hybridized: e.g., one of the variation operators in the USPEX evolutionary algorithm [5, 12, 13] essentially emulates metadynamics, and it is also possible to incorporate evolutionary search within metadynamics, as will be discussed later.

In this article we aim at presenting a brief review of the two recently developed algorithms, the metadynamics-based approach [6–8] and the evolutionary algorithm [5, 12]. The basic principles of both algorithms will be described and the application will be demonstrated on some examples with focus on systems relevant for geophysics. The article is organized as follows. In sections 2 and 3, we discuss metadynamics and its applications while in sections 4 and 5, we present the USPEX evolutionary algorithm and its applications. In the final section 6, we draw some conclusions and suggest possible directions of further developments.

2. Metadynamics-based approach

In this section we focus on methodological aspects of the metadynamics-based algorithm [6–8] which was constructed to enable simulations of structural phase transitions in crystals. Computer simulation of structural phase transitions is interesting on its own as it allows to uncover the mechanism of atomic rearrangements which bring the crystal from one structure to another. It thus offers a unique possibility since this information is hard to guess and difficult to extract directly from experiment. Knowledge of the transformation pathways can provide insight into the kinetics of phase transitions. Besides this motivation there is also an important connection to the crystal structure prediction problem – starting from one known crystal structure and changing external conditions the crystal may transform to

a new and previously unknown structure. Simulations of structural phase transitions in solids can thus have a predictive value. This was demonstrated for the first time by the Parrinello–Rahman method [14]. This method, based on the idea of a variable-cell constant-pressure MD, allowed simulations of structural transitions and particularly in combination with ab initio methods became a standard tool in theoretical investigation of structural transformations of both crystalline and amorphous solids (see Ref. [7] and references therein). However, a phase transformation can be observed in MD simulation only if the activation barrier is of the order $k_B T$ or less.

Structural phase transitions in solids are often first order as a consequence of the absence of a group–subgroup relation between the respective structures. It is well known that first-order transitions such as crystallization, melting and solid-solid transitions proceed generally via nucleation and growth which involves overcoming of an activation barrier. Proper and realistic simulations of such activated processes still remain a challenge because of the time and length-scale limitations of current simulation techniques. This is true even when a classical model potential is used and becomes considerably worse in case of an *ab initio* description.

Within the context of first-order transitions the solid-solid transitions represent a special case. In some cases these involve a reconstruction of the bonding pattern of the solid which itself might result in a large barrier. It is well known that even in experiment, many such transitions proceed on a slow time scale and many crystals persist in metastable state far above or below their thermodynamic transition pressure instead of converting to a thermodynamically stable state (diamond, silica [15]). The situation in computer simulations is even more difficult because for crystals one typically applies periodic boundary conditions which eliminate the surface. Since in small systems there are also no defects, this setup suppresses the possibility of a heterogeneous nucleation of a new phase. As a consequence, the transitions tend to proceed in a collective way which results in a barrier that can be substantially higher than the experimental one. Clearly, this makes the time-scale problem even worse. Any attempt to proceed towards more realistic simulations of structural transitions in crystals must therefore address the treatment of the activated process.

In Ref. [6] a new approach to this problem was proposed which is based on the metadynamics algorithm [16]. Recently this approach was further improved [8]. The new algorithm was successfully applied to a number of crystals of various kinds and proved to have much better predictive power than previous algorithms. The approach is based on the idea of exploration of the relevant thermodynamic potential in the space of a suitable order parameter. In the case of structural phase transitions a good candidate for such order parameter is the box matrix $\mathbf{h} = (\mathbf{a}, \mathbf{b}, \mathbf{c})$ (see Ref. [14]) where the vectors $\mathbf{a}, \mathbf{b}, \mathbf{c}$ are the three edges of the supercell. These vectors determine the periodicity of the system and the Gibbs free energy of a system consisting of a given number of atoms N can be expressed as a function of $\mathbf{h}$. When the atomic configuration corresponds to a stable or metastable crystal structure, the supercell must contain along each of the directions $\mathbf{a}, \mathbf{b}, \mathbf{c}$ an integer number of unit cells of the structure. Therefore the minima of the Gibbs free energy $\mathcal{G}(\mathbf{h}) = \mathcal{F}(\mathbf{h}) + PV$ ($\mathcal{F}$ is the Helmholtz free energy) are found for such values of $\mathbf{h}$ that are commensurate with the unit cell of a crystal structure which is stable or metastable at temperature T and pressure P. The problem of the simulation of structural transitions can then be formulated as the search for the lowest-energy path in the $\mathbf{h}$ space which brings the system from one minimum to another. As discussed in Refs. [6, 7] it is convenient to eliminate the three global rotational

degrees of freedom included in the 3×3 matrix $\mathbf{h}$. This is most easily done by rotating the system so that the matrix $\mathbf{h}$ becomes upper triangular. In this case it contains only six non-zero elements which can be represented by a 6D vector $\tilde{\mathbf{h}} = (h_{11}, h_{22}, h_{33}, h_{12}, h_{13}, h_{23})^T$.

The metadynamics algorithm is well suited for this kind of problem since it does not require the direct calculation of the free energy $\mathcal{G}(\mathbf{h})$. While this can be calculated in principle [17], the evaluation is cumbersome. Instead, in the metadynamics approach it is sufficient to calculate the first derivative of the free energy with respect to the order parameter. It can be easily shown that the derivative can be expressed as

$$-\frac{\partial \mathcal{G}}{\partial h_{ij}} = V\big[\mathbf{h}^{-1}(\mathbf{p} - P)\big]_{ji} \,, \tag{1}$$

which requires only the evaluation of the average pressure tensor $\mathbf{p}$ for a given box $\mathbf{h}$. This can be performed e.g., by a short MD simulation within the NVT ensemble.

Following the metadynamics algorithm [16], the exploration of the surface of the Gibbs free energy is performed by means of steepest-descent-like dynamics in the space of the $\tilde{\mathbf{h}}$ vector

$$\tilde{\mathbf{h}}^{t+1} = \tilde{\mathbf{h}}^{t} + \delta h \frac{\phi^{t}}{|\phi^{t}|}. \tag{2}$$

In the last expression, the driving force $\phi^t = -\partial G^t/\partial\tilde{\mathbf{h}}$ is derived from a modified Gibbs potential $\mathcal{G}^t$ which includes a history-dependent term

$$\mathcal{G}^{t}(\tilde{\mathbf{h}}) = \mathcal{G}(\tilde{\mathbf{h}}) + \sum_{t' < t} W e^{-(|\tilde{\mathbf{h}} - \tilde{\mathbf{h}}^{t'}|^2/2\delta h^2)}. \tag{3}$$

Here, a Gaussian has been added to $\mathcal{G}(\tilde{\mathbf{h}})$ at every point $\tilde{\mathbf{h}}^{t'}$ already visited in order to discourage the dynamics (equation (2)) from visiting it again. Therefore the force ϕ^t includes besides the thermodynamic driving force $\mathbf{F} = -(\partial\mathcal{G}/\partial\tilde{\mathbf{h}})$ also an additional term $\mathbf{F_g}$ arising from the history-dependent term. As the dynamics (equation (2)) goes on the Gaussians gradually fill the basin of attraction of the initial crystal structure and the system explores ever larger deformations. Since by construction these deformations are applied in order of increasing Gibbs free energy, the system eventually reaches the lowest free energy configuration where the initial structure is not stable anymore. At this point the atomic configuration enters into the basin of attraction of a new structure and undergoes a pronounced change which corresponds to the structural transformation. As the simulation continues the system first relaxes towards the bottom of the new free-energy well and when this is reached, it starts to fill the new well. In this way it is possible to observe within a single metadynamics simulation a series of transitions which may correspond either to several new structures or to a single transition proceeding via a number of (metastable) intermediate states. The metadynamics loop is performed until a transition occurs which can be often most easily detected by a visual inspection of the atomic configuration. If the entropic contribution to the Gibbs free energy can be neglected, enthalpy typically exhibits a pronounced drop when a transition takes place.

The above version of the algorithm was originally proposed in Ref. [6] and proven to work well for a number of systems [18–22]. Very recently an improvement of the technique was proposed [8]. It is well known that the energy cost of different deformations of crystals can vary significantly. The most costly deformations involve

changes in volume. On the other hand, deformations that conserve the volume such as shear or compression along one direction accompanied by elongation along a perpendicular direction can be performed at much lower energy cost. The shape of the free energy well in the $\tilde{\mathbf{h}}$ space is therefore highly anisotropic, similar to a valley having isolines in the shape of hyperellipsoids with their shortest semi-axis in the direction of volume change. Clearly, in order to explore such a landscape it would be ideal to use a Gaussian with δh proportional to the length of the respective semi-axis in each dimension. A symmetrical Gaussian on the other hand either drives the exploration too strongly into the direction of volume changes or takes too long to fill up the perpendicular directions. It is therefore useful to include some information about the shape of the initial well in the exploration of the free energy landscape.

The shape of the bottom of the free energy well can be characterized by expanding the Gibbs free energy up to the second order term around a given equilibrium crystal structure characterized by a matrix $\tilde{\mathbf{h}}^{\mathbf{0}}$. This can be written as

$$\mathcal{G}(\tilde{\mathbf{h}}) \approx \mathcal{G}(\tilde{\mathbf{h}}^{\mathbf{0}}) + \frac{1}{2}(\tilde{\mathbf{h}} - \tilde{\mathbf{h}}^{\mathbf{0}})^T \mathbf{A}(\tilde{\mathbf{h}} - \tilde{\mathbf{h}}^{\mathbf{0}}) \tag{4}$$

where the Hessian matrix

$$A_{ij} = \partial^2 \mathcal{G}(\tilde{\mathbf{h}})/\partial \tilde{h}_i \partial \tilde{h}_j \big|_{\tilde{\mathbf{h}}_0} \tag{5}$$

can be calculated from the pressure tensor using finite differences or from the $\mathbf{h}$ matrix fluctuations in a constant-pressure simulation. At equilibrium the $\mathbf{A}$ matrix has positive real eigenvalues $\{\lambda^i\}$ and can be diagonalized by an orthogonal matrix $\mathbf{O}$.

We now introduce new collective coordinates which bring all degrees of freedom in the 6D space of deformations to the same energy scale. Using the eigenvectors $\mathbf{O}$ and eigenvalues $\{\lambda^i\}$ we choose the new coordinates in the form

$$s_i = \sqrt{\lambda^i} \sum_j O_{ji}(\tilde{h}_j - \tilde{h}_j^0). \tag{6}$$

With this choice the well becomes spherical

$$\mathcal{G}(\mathbf{s}) \approx \mathcal{G}(\tilde{\mathbf{h}}^{\mathbf{0}}) + \frac{1}{2}\sum_i s_i^2. \tag{7}$$

The thermodynamic force in the new coordinates $\partial \mathcal{G}/\partial s_i$ is simply related to equation (1)

$$\frac{\partial \mathcal{G}}{\partial s_i} = \sum_j \frac{\partial \mathcal{G}}{\partial \tilde{h}_j} O_{ji} \frac{1}{\sqrt{\lambda^i}}. \tag{8}$$

The metadynamics simulation can then be performed in the s-coordinates in the same way as the original one [6] (equations (2) and (3)) (see Ref. [8]).

An important point is the choice of the Gaussian parameters δs and W which determine the resolution in the s space and in energy, respectively. It is hard to guess at the beginning what is the relevant scale of both quantities since no information about the landscape such as position and height of barriers is available. We require the two quantities δs and W to be related in such way that the curvature of the Gaussians is similar to the curvature of the free energy well. A similar prescription was used in Ref. [23]. In the s coordinates this condition can be simply stated as $W \sim \delta s^2$. In order to find the proper value of the Gaussian width δs it is useful first to

start with a large value of δs, e.g., one that is considerably larger than the thermal fluctuation $\delta s \gg \sqrt{k_B T}$ which usually results in some transition occurring within a few metasteps. Afterwards it is possible by choosing smaller values of δs to find a compromise between the resolution and CPU time. Clearly, small values of δs guarantee a very fine-grained exploration of the landscape but result in large number of metasteps necessary to fill the basin of attraction and observe a transition.

We note that this metadynamics approach is quite general and independent on the level of description of the system. It can be used with classical MD as well as with ab initio MD and in principle it can work also with MC simulation or Langevin dynamics etc. Since the exploration of the Gibbs free energy landscape is performed by means of a series of NVT simulations (an alternative continuous version of metadynamics is described in Ref. [24]), any MD code is suitable provided it calculates the stress tensor and allows for simulation of a crystal in a general non-orthorhombic box. There is no need to modify the integrator or any other part of the MD code and the algorithm can be simply implemented in the form of an external driver for the MD code. In figure 1 the organization of the metadynamics simulation is shown in the form of a flow chart. Each time the box matrix $\mathbf{h}$ is modified to a new value, $\mathbf{h}'$, the particle positions are rescaled in order to fit into the new box using the relation $\vec{r}' = \mathbf{h}'\mathbf{h}^{-1}\vec{r}$. The discrete first-order dynamics in the $\mathbf{h}$ space (equation (2)) does not accelerate when the system undergoes a structural transition, allowing the atomic configuration to adapt slowly and evolve into a new structure. Finally we note that some structural transitions can also be studied

start from an initial equilibrated structure $\mathbf{h}^0$, $\mathbf{r}^0$

MD code (NVT simulation)

read $\mathbf{h}^t$, $\mathbf{r}^t_{initial}$
equilibrate the system
average pressure tensor $\mathbf{p}^t$
write $\mathbf{h}^t$, $\mathbf{r}^t_{final}$, $\mathbf{p}^t$

Metadynamics code

read $\mathbf{h}^t$, $\mathbf{r}^t_{final}$, $\mathbf{p}^t$
calculate $\mathbf{h}^{t+1}$
get $\mathbf{r}^{t+1}_{initial}$ by rescaling $\mathbf{r}^t_{final}$ to $\mathbf{h}^{t+1}$
write $\mathbf{h}^{t+1}$, $\mathbf{r}^{t+1}_{initial}$
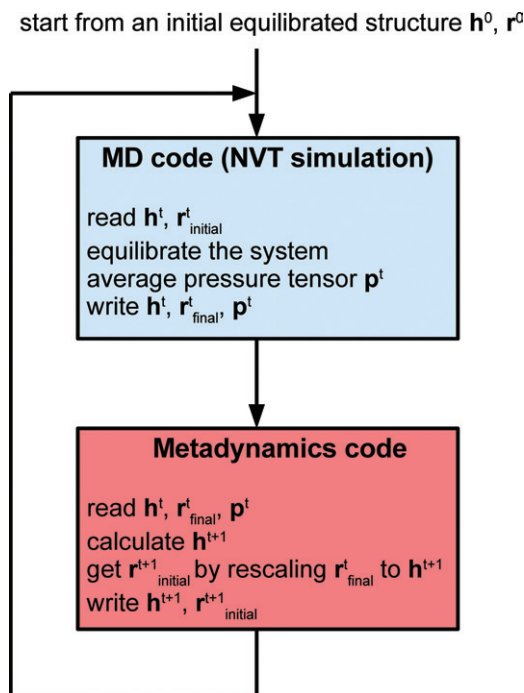
Figure 1. Flow chart of a metadynamics simulation showing the communication between the MD code and the metadynamics driver.

by metadynamics based on an order parameter different from the **h** matrix, as shown e.g., in Ref. [25], where a coordination number was used.

3. Results of metadynamics for various systems

The technique described in the previous section has been applied to several crystals such as silicon [6], zeolite [18], benzene [19], post-perovskite [20], phosphorus [21] and silica [8]. Besides inorganic and organic crystals it was also employed to study of a model core-softened pair potential [22]. Here we focus on two most recent applications to systems of geophysical interest, the study of the post-perovskite phase of $MgSiO_3$ and the study of transitions from 4- to 6-coordinated phases of SiO_2.

Probably the first application of *ab initio* metadynamics was to the geophysically important system $MgSiO_3$, the dominant component of the Earth's lowermost mantle. For a long time, researchers assumed that throughout the pressure–temperature regime of the lower mantle (24–136 GPa, 1800–4000 K, depths between 670 and 2890 km) the stable phase of $MgSiO_3$ has a perovskite-type structure. However, recently it was found that at conditions of the lowermost mantle, the so-called D'' layer (125–136 GPa, 2500–4000 K), a hitherto unsuspected $CaIrO_3$-type phase, called post-perovskite, becomes stable [26, 27]. Having an unusual layered structure (figure 2), post-perovskite has a number of unusual properties that successfully explained most of the geophysical anomalies associated with the D'' layer. At first, the perovskite and post-perovskite structures seem to be completely different.
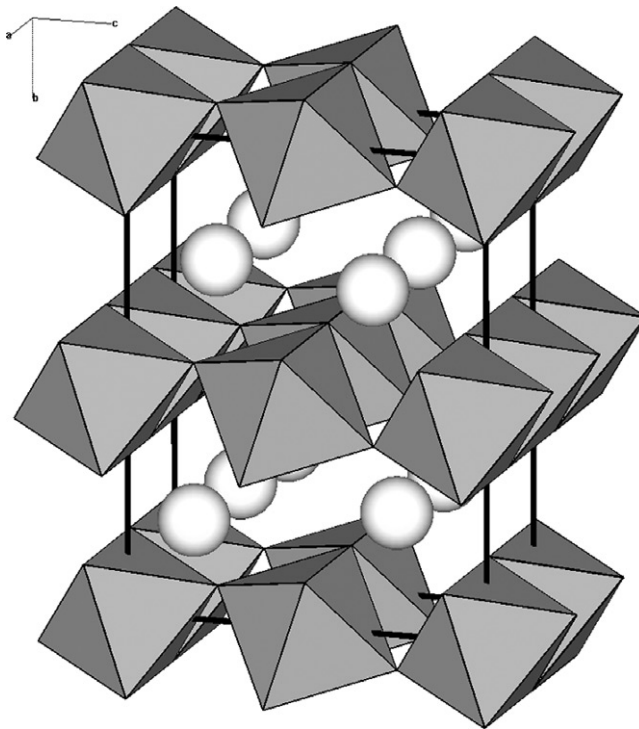
Figure 2. $CaIrO_3$-type structure of post-perovskite (after [26]).
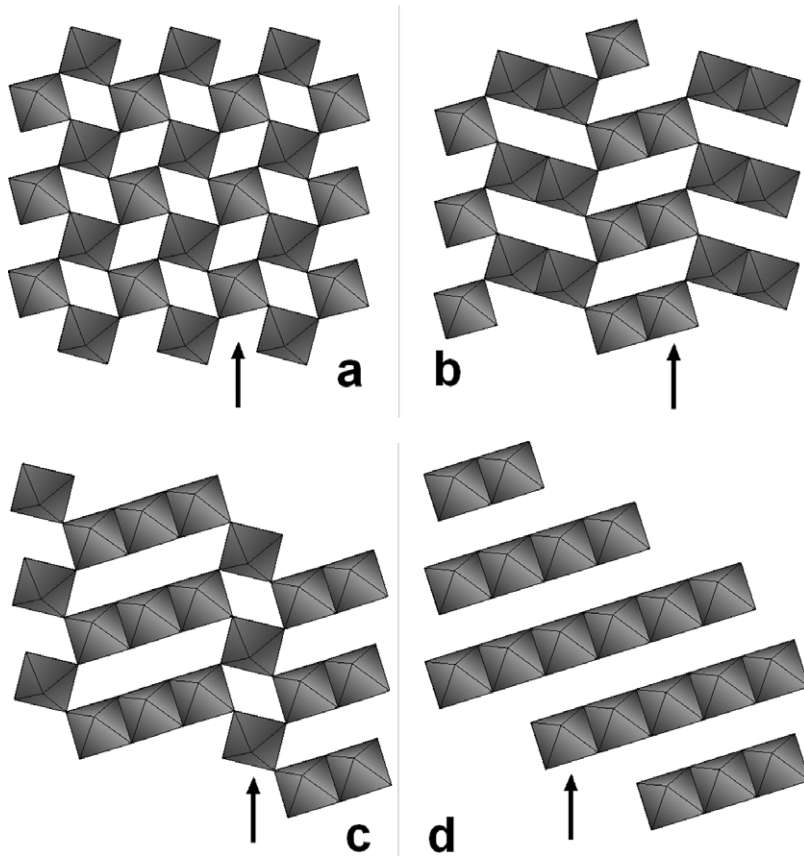
Figure 3. MgSiO$_3$ polytypes [20]: a – perovskite (space group *Pbnm*), d – post-perovskite (*Cmcm*), b, c – newly found structures 2×2 (*Pbnm*) and 3×1 (*P2$_1$/m*), respectively. Only silicate octahedra are shown; Mg atoms are omitted for clarity. In the post-perovskite structure, the predicted plastic slip plane {110} is shown by an arrow. Arrows also show the likely slip planes in the other structures.

Metadynamics simulations [20] brought much new insight (here the earlier version of the algorithm using directly the **h** matrix as the collective coordinate was employed). They revealed that the two structures are closely related and can be considered as end members of an infinite polytypic series (figure 3). The intermediate polytypes (figure 3, table 1) are energetically very close to perovskite and post-perovskite and could be stabilized by temperature and Fe–Al–Ca impurities (abundantly present in the mantle) and become stable mantle minerals. These polytypes have diffraction patterns intermediate between perovskite and post-perovskite, but with additional peaks; such new peaks were recently observed in experiments on chemically impure MgSiO$_3$ [28]. According to metadynamics simulations, the perovskite – post-perovskite transition is likely to proceed by plane sliding involving these intermediate structures, and so is plastic deformation of both minerals. Oganov *et al.* in Ref. [20] showed that in post-perovskite the {110} planes (the plane of stacking faults) should be the dominant planes of plastic slip. The slip plane determines the texture of minerals in the D″ layer and creates its anisotropic properties.

Table 1.   Structural data on perovskite – post-perovskite polytypes of MgSiO$_3$ at 120 GPa.

Perovskite. Space group *Pbnm*.
$a = 4.318$ Å, $b = 4.595$ Å, $c = 6.305$ Å

Mg	0.5246	0.5768	0.25
Si	0.5	0	0.5
O1	0.1164	0.4669	0.25
O2	0.1829	0.1926	0.5575

3×1-structure. Space group $P2_1/m$.
$a = 4.256$ Å, $b = 6.221$ Å, $c = 9.478$ Å, $\beta = 98.74°$

Mg1	0.0734	0.75	0.3036
Mg2	0.8940	0.75	0.8000
Mg3	0.0122	0.25	0.4412
Mg4	0.4572	0.25	0.9573
Si1	0	0	0
Si2	0.5	0	0.5
Si3	0.5836	0.0011	0.2474
O1	0.4511	0.75	0.2290
O2	0.7169	0.25	0.2655
O3	0.8848	0.25	0.0161
O4	0.6362	0.25	0.5203
O5	0.3547	0.0589	0.0938
O6	0.8025	0.9428	0.4069
O7	0.8760	0.9396	0.1555
O8	0.2824	0.0572	0.3424

2×2-structure. Space group *Pnma*.
$a = 4.252$ Å, $b = 9.368$ Å, $c = 6.225$ Å

Mg1	0.5578	0.0712	0.25
Mg2	0.6233	0.1732	0.75
Si	0.0819	0.1276	0.9969
O1	0.9587	0.1446	0.25
O2	0.2116	0.1077	0.75
O3	0.4090	0.2176	0.0612
O4	0.2493	0.9691	0.0559

Post-perovskite. Space group *Cmcm*.
$a = 2.474$ Å, $b = 8.121$ Å, $c = 6.138$ Å

Mg	0	0.2532	0.25
Si	0	0	0
O1	0	0.927	0.25
O2	0	0.6356	0.4413

The {110} slip planes provided a new interpretation of the seismic anisotropy of the D'' layer [20], which appears to be very robust. Recent seismological observations (Ref. [29]) gave further strong support to this interpretation.

The next example we show here is the study of structural transformations in crystalline silica [8] which is also of great interest for geophysics as well as for materials science. It is well known that 4-coordinated phases of silica at room temperature have a tendency to amorphize under pressure [15]. Moreover, the outcome of the experiment is strongly dependent both on the initial structure and on the pressurization protocol [15, 30]. Both experimental and theoretical study of this system therefore represent a challenge and previous simulations could not reproduce
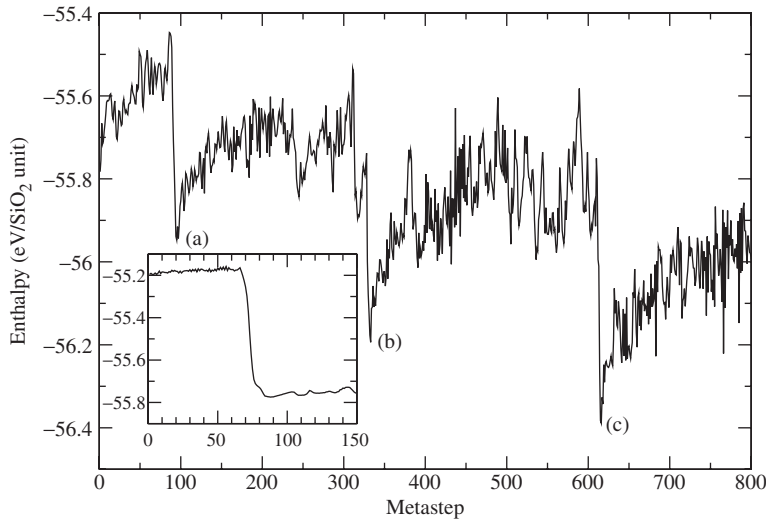
Figure 4.   Evolution of the enthalpy in the simulation starting from the quartzII. In the inset the enthalpy during the simulation starting from α-quartz is shown. Simulation was performed at $T = 300\,\text{K}$ and $p = 150\,\text{kbar}$. After Ref. [8].

all phases observed in experiments. In this work the new version of the algorithm using the transformed collective coordinates (equation (6)) was employed since the improved sampling of the free energy surface substantially helps to avoid amorphization.

The structural transformations starting from α-quartz were studied using the 324-atom supercell and the classical BKS potential [31]. The simulation was performed at $T = 300\,\text{K}$ and $p = 150\,\text{kbar}$. As shown in Ref. [32], at these conditions the stable phase is the 6-coordinated stishovite structure. The evolution of the enthalpy of the system (which in this case is a good approximation of the Gibbs free energy) is shown in figure 4. The inset shows the initial phase where α-quartz transforms into quartzII, which is seen as a pronounced drop of the enthalpy. Subsequently, the simulation, starting from the quartzII structure, proceeds via crossing of several large barriers (figure 4), bringing the system first to a defective octahedrally coordinated structure and later into a perfect octahedral structure consisting of 3×2 kinked chains of edge-sharing octahedra. This structure (space group $P2_1/c$) was observed in the experiment [33] and belongs to a generic family of high-pressure silica structures [34] consisting of chains of edge-sharing octahedra with various degrees of kinking. The final transition brings the system to stishovite which consists of straight chains of octahedra. This phase was observed, although poorly crystallized, in experiment upon pressurization of α-quartz beyond $600\,\text{kbar}$ [35]. In figure 5 it can be seen how the 3×2 kinking pattern is eliminated in two steps, proceeding via intermediate state with 6×2 kinking pattern and finally resulting in straight chains with no kinks. The transition mechanism involves octahedra which during the bond switching process temporarily share their corners instead of edges. The metadynamics simulations succeeded in this case in bringing simulations much closer to experiment.
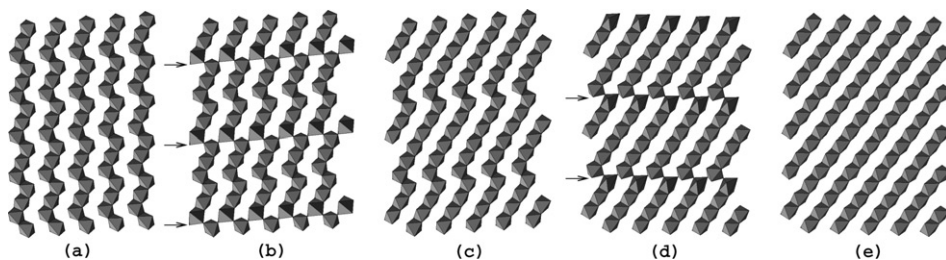
Figure 5. SiO$_2$: two steps of the transition from the 3×2 structure (a) to stishovite (e). Elimination of the kinking of octahedral chains proceeds via an intermediate 6×2 structure (c). The arrows denote the presence of corner-sharing octahedra in the transition states (b) and (d). After Ref. [8].
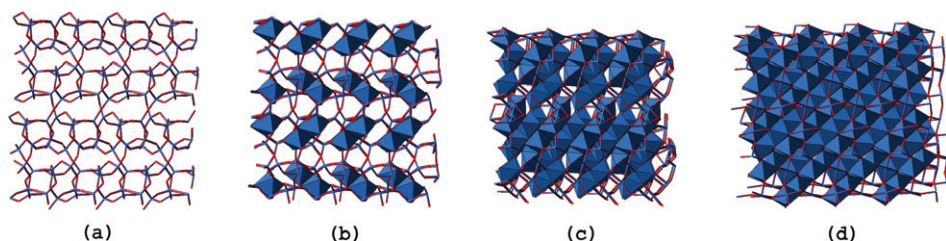
Figure 6. Structural evolution during the transition from coesite (a) to the α-PbO$_2$ phase (d). Intermediate states (b) and (c) show the initial growth and competition of chains of octahedra in different planes. After Ref. [8].

The other case studied in Ref. [8] was the pressure-induced transformation starting from coesite, which was found to amorphize under application of pressure at room temperature, both in experiment and in simulation [30, 36]. A 48-atom super-cell of coesite was simulated at pressure of 220 kbar and $T = 600$ K using *ab initio* Car–Parrinello [37] MD for metadynamics. We observed a direct transformation of coesite to the metastable α-PbO$_2$ structure. The structural evolution during this transition is shown in figure 6. As such a transition has so far not been observed in the experiment, in this case the metadynamics simulations succeeded in providing a new prediction. Moreover, since the dominant change of the supercell geometry across the transition is the shrinkage of the b axis by about $\sim 15\%$, it is likely that application of a uniaxial compression along the b axis to coesite should favour the transition to the α-PbO$_2$ structure.

4. Evolutionary crystal structure prediction

The evolutionary algorithm developed by Oganov and Glass [5, 13] has been implemented in the USPEX (Universal Structure Predictor: Evolutionary Xtallography) code – for the most detailed description see Ref. [13]. Unlike most methods of crystal structure prediction, USPEX requires no initial structure and no experimental information at all. The only input is the number of atoms of each sort, pressure–temperature conditions and parameters of evolution (such as the

probabilities of heredity and mutations). The high efficiency of the algorithm makes it possible to perform purely *ab initio* structure prediction at reasonable computational cost. Numerous tests showed the excellent performance of the algorithm [5].

The algorithm looks for the global minimum of the free energy at given pressure–temperature conditions. In most applications of USPEX so far, structure prediction was done starting with randomly produced structures (though starting with known structures is also possible). The free energy surface is rough and has a very large number of local minima separated by high energy barriers. To make the search for the global minimum feasible, it is essential to locally optimise all candidate structures during the simulation. The so-called reduced response surface [13] – i.e., the free energy surface reduced to the local minima – has a much clearer overall shape than the original free energy surface. Within each generation, the free energies of locally optimised structures are compared and a certain percentage of the lowest-energy structures are used to create (through heredity and various types of mutation) a new generation of structures. During the simulation, the algorithm "learns" energetically favourable atomic arrangements and, creating new structures from these, effectively zooms in on the promising parts of the free energy surface.

The key is to ensure that the representation of structures and the variation operators (heredity and mutations), on the one hand, optimally incorporate structural information learned from low-energy structures and, on the other hand, sufficient structural diversity is maintained throughout the simulation (allowing new solutions to be found and avoiding "sticking" to local minima). Structures (lattice vectors and atomic coordinates) are represented by floating-point numbers, rather than binary strings; scale-invariant fractional atomic coordinates are used. During heredity, new structures are produced by matching spatially coherent slabs (chosen in random directions and with random positions) of parent structures. Heredity for the lattice vectors matrix (represented in the upper-triangular form to avoid unphysical whole-cell rotations) is done by taking a weighted average, with a random weight. The permutation operator (needed only when there are two or more types of atoms) swaps identities of two or more atoms in the structure, thus helping to find optimal atomic ordering. In lattice mutation each mutated cell vector $\mathbf{a}'$ is defined as a product of the old vector ($\mathbf{a^0}$) and the $(\mathbf{I} + \epsilon)$ matrix:

$$\mathbf{a}' = (\mathbf{I} + \epsilon)\mathbf{a^0} \tag{9}$$

where $\mathbf{I}$ is the unit matrix and ϵ is the symmetric strain matrix, so that:

$$(\mathbf{I} + \epsilon) = \begin{pmatrix} 1 + \epsilon_1 & \epsilon_6/2 & \epsilon_5/2(11) \\ \epsilon_6/2 & 1 + \epsilon_2 & \epsilon_4/2(12) \\ \epsilon_5/2 & \epsilon_4/2 & 1 + \epsilon_3 \end{pmatrix} \tag{10}$$

The strain matrix components are drawn randomly from the Gaussian distribution and can take values between -1 and 1. Lattice mutation essentially incorporates the ideas of metadynamics into USPEX. However, metadynamics finds new structures by building up cell distortions of some known structure, and in USPEX the distortions are not accumulated and to yield new structures the strain components should be large. Finally, a specified number of the best structures (usually, one) in the current generation survive into the next generation ("survival of the fittest") – apart from a generally beneficial effect on the population, this guarantees a variational property that the lowest free energy in each generation can only decrease or
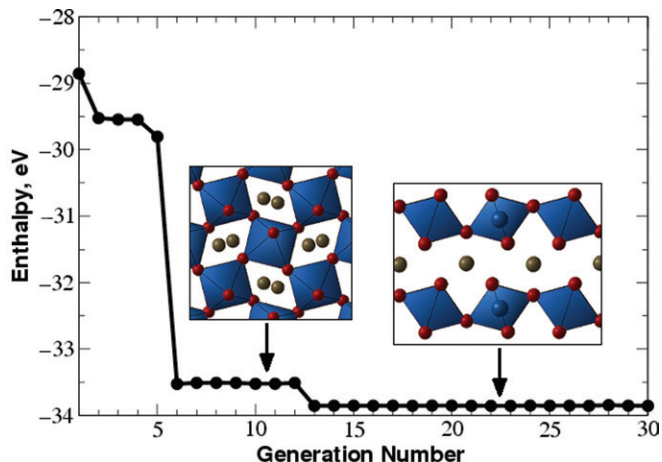
Figure 7. Example of an *ab initio* evolutionary run: 20-atom variable-cell simulation of $MgSiO_3$ at 120 GPa and 0 K. The lowest enthalpy in each generation is shown as a function of generation number (each generation contains 30 structures). Without any experimental information and starting with random structures, the simulation discovers the perovskite structure at 6th generation, and the post-perovskite phase (stable at 120 GPa) at 13th generation. From Ref. [5].

stay constant through progressive generations. The simulation is terminated once the lowest free energy showed no change after sufficiently many generations. In our experience, for systems with ~20 atoms in the cell finding the stable crystal structure usually takes up to ~20 generations (figure 7).

The power of USPEX can be further demonstrated by comparing the performance of USPEX and a simple non-learning algorithm involving random sampling and local optimisation of all structures. The test was done for $MgSiO_3$ post-perovskite, trying to reproduce the calculations described in Ref. [27] as leading to a solution of the post-perovskite structure. These authors quenched randomly generated structures using molecular dynamics quenches of random structures (similar to local optimization of randomly produced structures, performed here) to find the structure. We used the same doubled 40-atom cell with experimental cell parameters of post-perovskite at 125 GPa, and the same interatomic potential. Local optimisations were done using the GULP code [38]. Strikingly, locally optimising more than 10^5 random structures did not yield the post-perovskite structure – the best structure obtained in this way is 1.02 eV/cell higher in energy. The probability of finding even this structure with random sampling is extremely low (figure 8, top). This structure can be transformed into post-perovskite through Mg–Si permutation and is probably what was actually found by Murakami *et al.* [27], who as noted by Hirose *et al.* [39] applied to it an "artificial" Mg–Si exchange to arrive at the post-perovskite structure [56]. Given the extremely low probability of finding this structure at zero Kelvin, it is surprising that it was found (Ref. [39]) in five out of ten molecular dynamics quenches (this can be reconciled with our results only if most energy barriers between structures are small enough to be overcome in molecular dynamics). Unlike random sampling, USPEX found the correct post-perovskite structure and needed fewer than 500 local optimisations (12 generations) to do so. Starting with random structures (which have the same distribution of energies as shown on top of figure 8), the
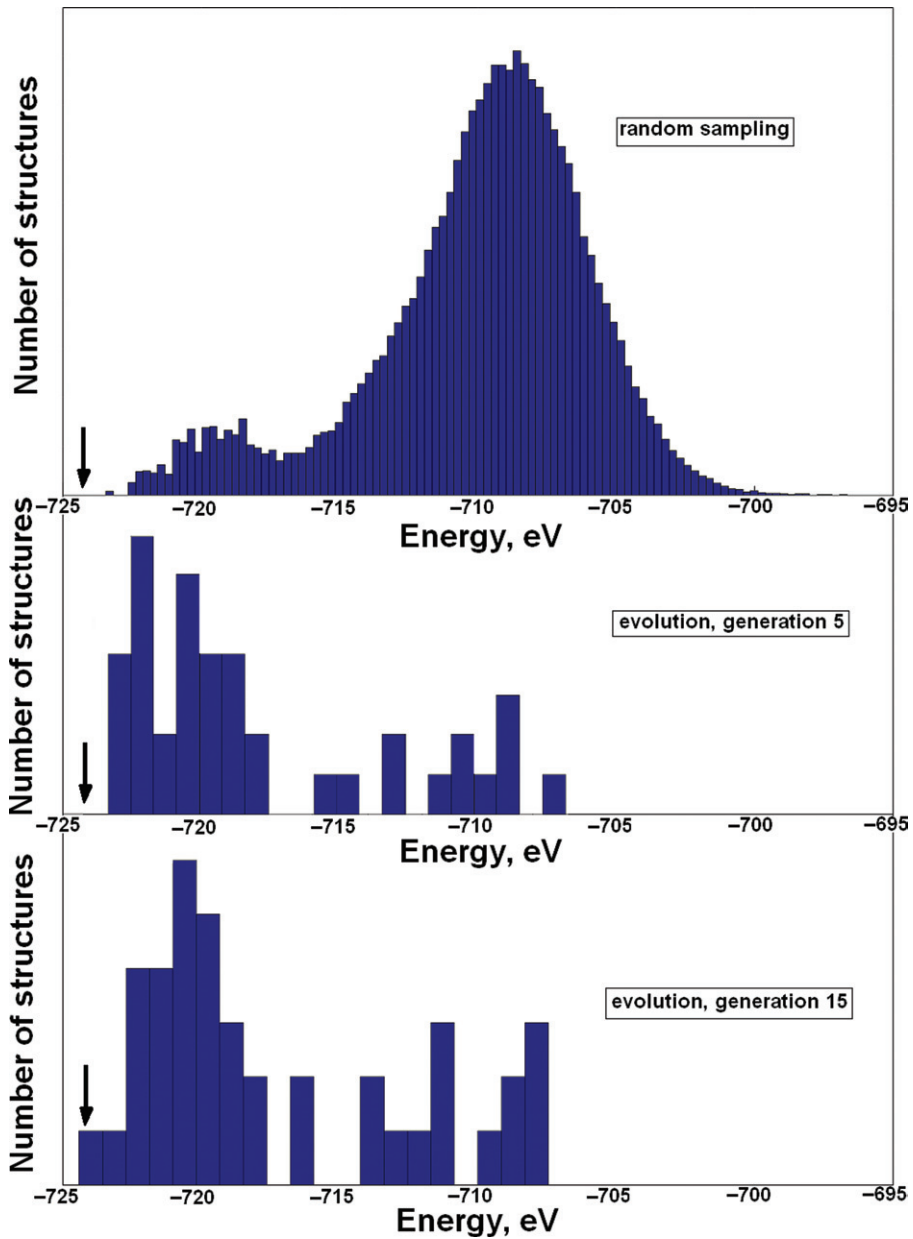
Figure 8. Sampling of the energy surface: comparison of random sampling and evolutionary algorithm for a 40-atom cell of $MgSiO_3$ with cell parameters of post-perovskite. In all cases, energies of locally optimized structures are shown. For random sampling, 10^5 structures were generated (none of them corresponded to the ground state). For evolutionary search, each generation included 40 structures (the first generation being produced randomly) and the ground-state structure was found within 15 generations. The energy of the ground-state structure is indicated by the arrow. This picture shows that "learning" incorporated in evolutionary search drives the simulation towards lower-energy structures.
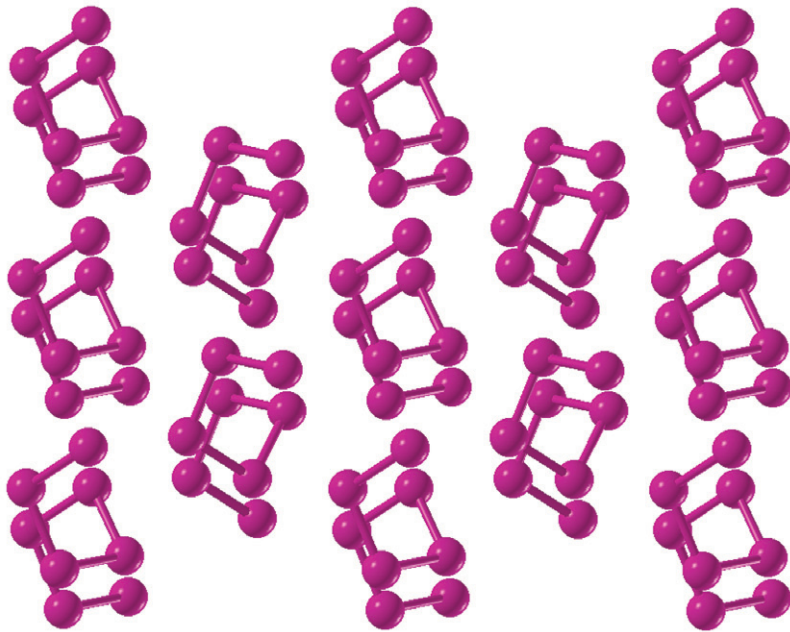
Figure 9.   Newly predicted $P2_12_12_1$ structure of sulphur, found by USPEX (after Ref. [5]).

algorithm learned how to produce low-energy structures and the distribution of energies very quickly started to gravitate towards low energies while keeping sufficient diversity and spread of energies (figure 8, middle and bottom).

5. Results of evolutionary simulations

Several important new results obtained with USPEX have been described in Refs. [12, 5]; here we briefly discuss only three cases – new high-pressure phases of sulphur, $CaCO_3$ and structures of carbon at 0–2000 GPa. All these examples were studied using *ab initio* calculations within the generalized gradient approximation [40].

   Elemental sulphur is known [41] to exhibit a large number of crystalline phases, but only five phases have been demonstrated to be stable up to 90 GPa: α-S and β-S (both based on S_8 crown ring molecules) at 1 atm and up to $\sim$3 GPa, and three phases in the pressure range $\sim$3–90 GPa [42–45]. Among the three high-pressure structures, one is based on S_6 crown ring molecules, one contains trigonal spiral chains of sulphur atoms and the other has tetragonal spiral chains. USPEX simulations at 12 GPa produced all these three phases, a large number of low-energy metastable structures, and one additional new structure based on distorted tetragonal spiral chains of sulphur atoms and having the space group $P2_12_12_1$ (figure 9). Within the generalized gradient approximation [40], this structure is stable up to 7 GPa [5]. Like all the other stable structures of sulphur, this structure is well described by the "8-N" rule: the coordination number of the atom is equal to eight minus the number of the element's group in the Periodic Table. This rule is
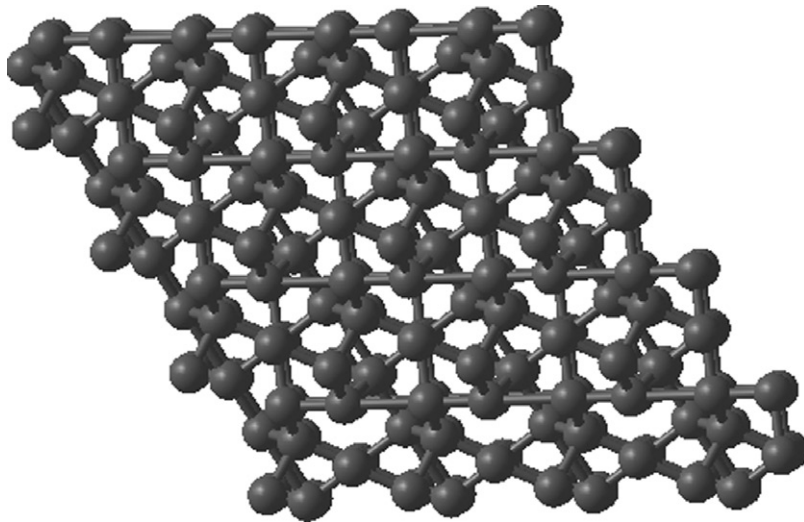
Figure 10. bc8 structure of carbon, stable above 1000 GPa and produced by USPEX (after Ref. [5]).

fulfilled for crystals with ordinary covalent bonds, and sulphur clearly belongs to this class of structures up to the pressure of its metallization ($\sim$90 GPa).

For carbon, it is well known that the stable low-pressure phase is graphite, and above $\sim$5 GPa diamond is stable. It has been suggested [46] that the so-called bc8 structure (found to be metastable for Si [47], see figure 10) becomes stable above $\sim$1000 GPa. Carbon atoms have sp^2 hybridisation in graphite, but sp^3 hybridisation in higher-pressure diamond and bc8 structures (the latter is metallic in its stability field and has carbon in a heavily distorted tetrahedral coordination). USPEX simulations were performed at 1 atm, 100 GPa, 1000 GPa and 2000 GPa [5] and found all these structures. These simulations clearly showed stability of graphite at 1 atm, diamond at 100 GPa, and bc8 phase at 2000 GPa; at 1000 GPa diamond and bc8 phase had practically identical enthalpies and were both found in the same simulation. Thus, our results strongly support the "traditional" sequence graphite-diamond-bc8 with increasing pressure. The phase transition diamond-bc8 at 1000 GPa puts an upper limit in pressure to the diamond-anvil cell technique for studies of matter at high compressions. In these simulations, several interesting metastable structures were found, some previously known and some unknown. Among the known metastable structures identified in USPEX runs are lonsdaleite ("hexagonal diamond", figure 11a) found at 100 GPa and an interesting "5 + 7" structure (figure 11b) that actually corresponds to the (2×1) reconstruction of the (111) surfaces of diamond and silicon (we also found this structure as metastable in runs for silicon at 1 atm). The low-energy metastable structures at 1 atm included various layered (including a 2-dimensional analogue of the "5 + 7" structure) and chain structures, as well as two unique 3-dimensional structures combining stripes of the graphite structure and layers of the diamond structure (figure 11c) and graphite stripes in two orientations (figure 11d). These structures are most likely to possess unique mechanical and electrical properties; they are 0.4–0.5 eV/atom less favourable than graphite – i.e. only twice more unfavourable than diamond at 1 atm and thus potentially synthesizable. In particular, the structure made of graphite stripes has
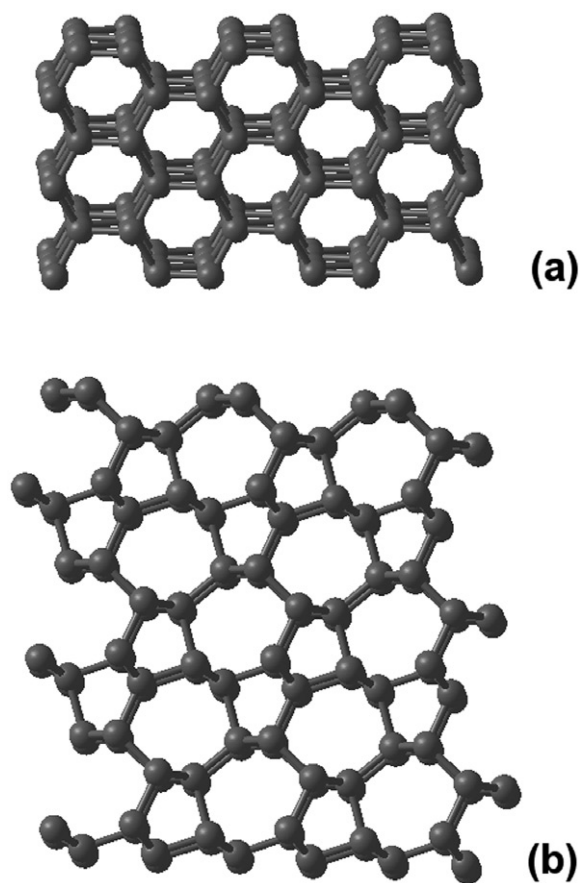
Figure 11. Metastable phases of carbon produced by USPEX – (a) lonsdaleite, (b) "5 + 7" structure, (c–d) "stripe" structure containing carbon in sp^2 and sp^3 hybridisation, and only sp^2 hybridisation, respectively (after Ref. [5]).

stronger C–C bonds than in diamond and unlike graphite is fully 3-dimensional and could therefore have an unprecedented hardness.

An important question in Earth sciences is the mineralogical reservoir of carbon inside the Earth. As solubility of carbon in mantle silicates is very low [48], the Earth's carbon is likely to be concentrated in the form of Mg and Ca carbonates, perhaps CO_2, and to a smaller extent diamond. A new phase of $CaCO_3$ (named post-aragonite) was found to be stable above 40 GPa by Ono *et al.* [49]; however, the structure could not be solved from experimental data. Using USPEX, the structure was solved [12], shown to be stable above 42 GPa and proved to match well all the experimental data. The structure type of post-aragonite (figure 12a) has not been previously known and is extremely interesting: it contains coplanar CO_3-triangles and Ca atoms in the 12-fold coordination; the structure can be alternatively described as based on the hexagonal close packing of calcium and oxygen atoms (explaining the high density of the structure), with carbon atoms occupying trian-gular voids. As of today, we know the same post-aragonite structure to be stable also for $SrCO_3$ and $BaCO_3$ at high pressure [50]. In the same theoretical study [12] it was found with USPEX that above 137 GPa a new phase of $CaCO_3$ should be stable.
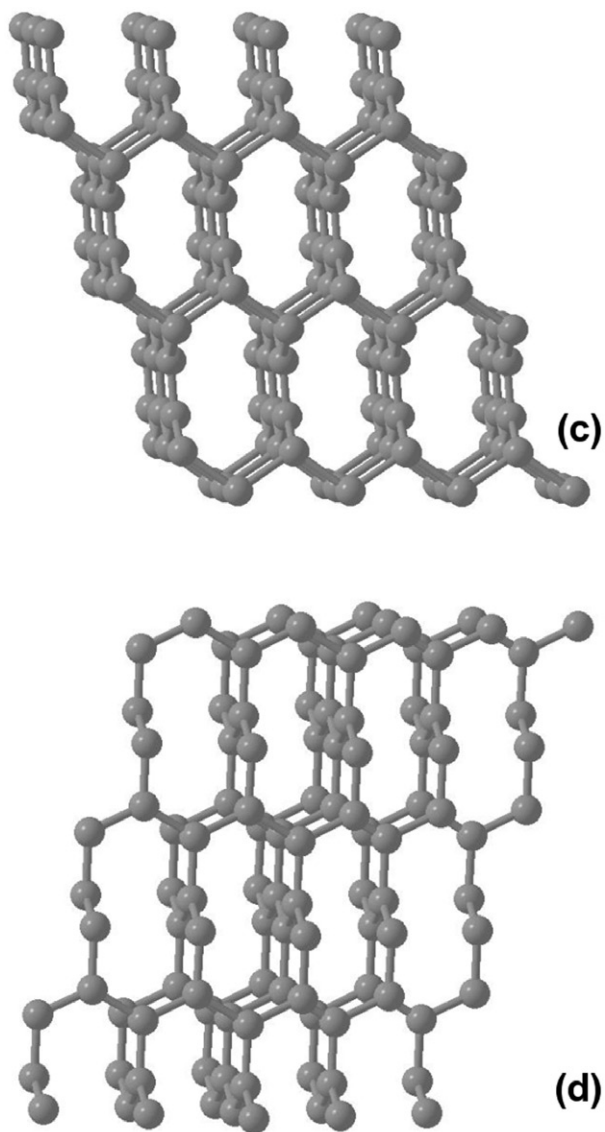
Figure 11.   Continued.

This phase also has a unique structure (figure 12b), not previously observed for any compound. This structure contains chains of corner-sharing tetrahedral carbonate ions CO_4^{4-} (instead of the isolated CO_3^{2-} triangular ions experimentally known up to now). Several months after the original prediction [12] this phase was verified experimentally [50].

6. Conclusions

We have presented two recent approaches, metadynamics and an evolutionary algorithm, which can be applied to study of crystal structure transformations and
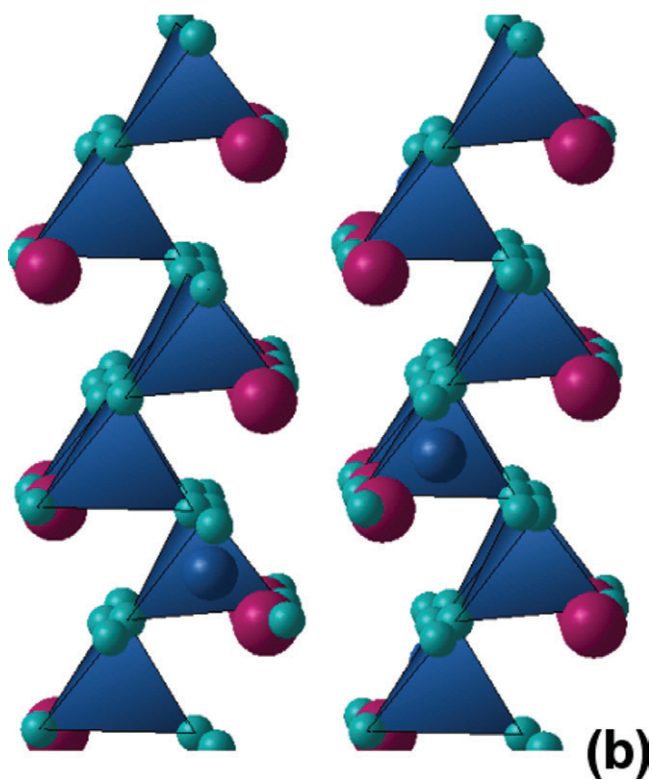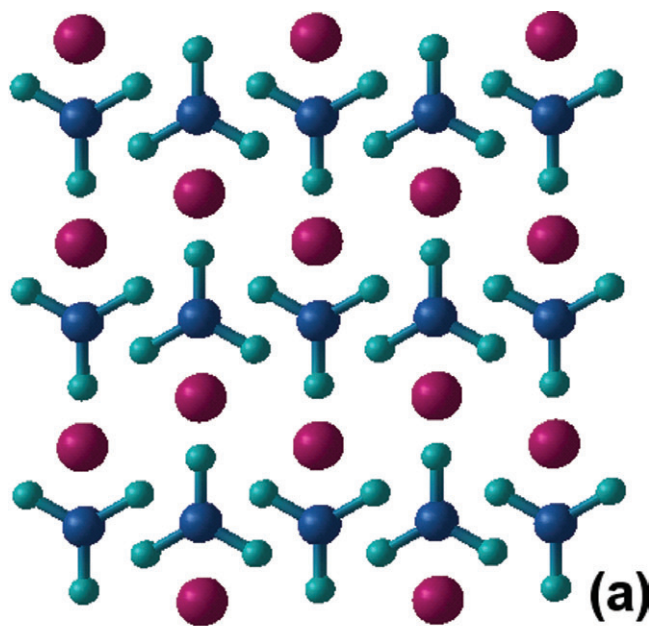
Figure 12. High-pressure phases of CaCO$_3$ found by USPEX: (a) post-aragonite, (b) "post-post-aragonite" $C2221$ phase (after Refs. [12, 5]).

crystal structure prediction. Both approaches can be seen as complementary and can also be combined at various levels. For example, it might be interesting to run metadynamics at $T = 0$ and use the evolutionary algorithm as optimization algorithm to find for each value of the order parameter (the box matrix **h**) the corresponding atomic or molecular configuration.

The metadynamics-based approach proved to be a definite step forward in the study of structural transitions, substantially increasing the predictive power of simulations and bringing them much closer to experiment. Still, further developments are possible and desirable. As discussed in section 2, the use of supercell vectors which act as order parameter tends to favour a collective mechanism for the transition (for more details see Ref. [7]). Proper simulation of nucleation in solid–solid phase transitions is notoriously complicated and requires further algorithmic development. First steps in this direction were taken by Zahn and Leoni [51, 52] applying the transition path sampling method [53]. This technique is capable of finding a more realistic transition mechanism provided both the initial and final structures are known. In order to achieve a fully realistic simulation one would need to simulate a very large system, containing extended defects such as dislocations which are likely to play an important role in the nucleation process. Realistic simulations of structural transitions in crystals therefore still represent a challenge.

With the evolutionary algorithm USPEX, a new level of crystal structure prediction has been achieved. Not only can one predict (efficiently and reliably) the stable phase at given conditions, but there is also now an access to a wealth of complementary chemical information from a large set of low-energy metastable structures. During USPEX simulations, the algorithm continuously ''learns'' from low-energy structures about the favourable atomic arrangements. This information can be uncovered in the analysis of simulation results, leading to a richer understanding of the structural chemistry of the element/compound and its response to changes in pressure and temperature. This information can be used to understand the rules governing the stability of crystal structures.

The main limitations of both methods include: (1) aperiodic systems (for which a periodic approximant would be produced), (2) disordered systems (for which the lowest-energy ordered variant will be produced), (3) systems with very large unit cells (both methods have demonstrated good performance for systems with up to several hundred atoms per cell), (4) reliance on approximations (approximate forcefields or exchange-correlation functionals), but increasingly accurate approximations are becoming available. Only the limitation 3 is intrinsic to metadynamics and evolutionary algorithms themselves (but there is active work now to extend the method to very large systems). Limitations 1, 2, 4 come from the underlying free-energy calculations, but rapid progress in *ab initio* simulation methodologies gives much hope that these limitations will also be reduced or removed.

support of this work, and S. Ono, J. Wookey, O. Tschauner for useful discussions. Calculations have been performed at ETH Zurich and CSCS (Manno). We thank T. Racic, G. Sigut, S. Mauri, O. Byrde, and N. Stringfellow for technical support of the calculations. CWG thanks his dear friend Jo A. Helmuth for many fruitful discussions.

References

[1] J. Pannetier, J. Bassasalsina, J. Rodriguez-Carvajal, *et al.* Nature **346** 343 (1990).
[2] J. Schön and M. Jansen, Angew. Chem. Int. Ed. **35** 1287 (1996).
[3] T. Bush, C. Catlow and P. Battle, J. Mater. Chem. **5** 1269 (1995).
[4] P. Ball, Nature **381** 648 (1996).
[5] A. Oganov and C. Glass, J. Chem. Phys. **124** 244704 (2006).
[6] R. Martoňák, A. Laio and M. Parrinello, Phys. Rev. Lett. **90** 075503 (2003).
[7] R. Martoňák, A. Laio, M. Bernasconi, *et al.*, Z. Kristallogr. **220** 489 (2005).
[8] R. Martoňák, D. Donadio, A.R. Oganov and M. Parrinello, Nature Mater. **5** 623 (2006).
[9] D. Wales and J. Doye, J. Phys. Chem. **A101** 5111 (1997).
[10] S. Gödecker, J. Chem. Phys. **120** 9911 (2004).
[11] S. Woodley, Struct. Bond. **110** 95 (2004).
[12] A. Oganov, C. Glass and S. Ono, Earth Planet Sci. Lett. **241** 95 (2006).
[13] C.W. Glass, A.R. Oganov and N. Hansen, Comp. Phys. Comm. **175** 713 (2006).
[14] M. Parrinello and A. Rahman, Phys. Rev. Lett. **45** 1196 (1980).
[15] R.J. Hemley, C.T. Prewitt and K.J. Kingma, *Silica – Physical Behaviour, Geochemistry and Materials Applications* (Mineral Soc. of Am., Washington DC, 1994), Vol. 29 of Rev. Mineral., chap. High-pressure behaviour of silica, p. 41.
[16] A. Laio and M. Parrinello, Proc. Natl. Acad. Sci. USA **99** 12562 (2002).
[17] D. Frenkel and B. Smit, *Understanding Molecular Simulation* (Academic Press, London, 2002).
[18] C. Ceriani, A. Laio, E. Fois, *et al.*, Phys. Rev. B **70** 113403 (2004).
[19] P. Raiteri, R. Martoňák and M. Parrinello, Angew. Chem. Int. Ed. **44** 3769 (2005).
[20] A.R. Oganov, R. Martoňák, A. Laio, *et al.*, Nature **438** 1142 (2005).
[21] T. Ishikawa, H. Nagara, K. Kusakabe, *et al.*, Phys. Rev. Lett. **96** 095502 (2006).
[22] D. Quigley and M.I.J. Probert, Phys. Rev. E (Stat., Nonlin. Soft Matter Phys.) **71** 065701 (2005).
[23] H. Grubmüller, Phys. Rev. E **52** 2893 (1995).
[24] M. Pagliai, M. Iannuzzi, G. Cardini, *et al.*, Chemphys. Chem. **7** 141 (2006).
[25] F. Zipoli, M. Bernasconi and R. Martoňák, Eur. Phys. J. B **39** 41 (2004).
[26] A. Oganov and S. Ono, Nature **430** 445 (2004).
[27] M. Murakami, K. Hirose, K. Kawamura, *et al.*, Science **304** 855 (2004).
[28] O. Tschauner, personal communication.
[29] J. Wookey, personal communication.
[30] R.J. Hemley, A.P. Jephcoat, H.K. Mao, *et al.*, Nature **334** 52 (1988).
[31] B.W.H. van Beest, G.J. Kramer and R.A. van Santen, Phys. Rev. Lett. **64** 1955 (1990).
[32] I. Saika-Voivod, F. Sciortino, T. Grande, *et al.*, Phys. Rev. E **70** 061507 (2004).
[33] J. Haines, J.M. Léger, F. Gorelli, *et al.*, Phys. Rev. Lett. **87** 155503 (2001).
[34] D.M. Teter, R.J. Hemley, G. Kresse, *et al.*, Phys. Rev. Lett. **80** 2145 (1998).
[35] Y. Tsuchida and T. Yagi, Nature **347** 267 (1990).
[36] D.W. Dean, R.M. Wentzcovitch, N. Keskar, *et al.*, Phys. Rev. B **61** 3303 (2000).
[37] R. Car and M. Parrinello, Phys. Rev. Lett. **55** 2471 (1985).
[38] J. Gale, Z. Kristallogr. Rev. Geophys. **220** 552 (2005).
[39] K. Hirose, Rev. Geophys. **44** RG3001 (2006).
[40] J.P. Perdew, K. Burke and M. Ernzerhof, Phys. Rev. Lett. **77** 3865 (1996).
[41] G. Vezzoli, F. Dachille and R. Roy, Science **166** 218 (1969).
[42] W. Crichton, G. Vaughan and M. Mezouar, Z. Krist. **216** 417 (2001).
[43] H. Fujihisa, Y. Akahama, H. Kawamura, *et al.*, Phys. Rev. B **70** 134106 (2004).
[44] L. Crapanzano, W. Crichton, G. Monaco, *et al.*, Nat. Mater. **4** 550 (2005).

[45] O. Degtyareva, E. Gregoryanz, H. Mao, *et al.*, High Pres. Res. **25** 17 (2005).
[46] S. Fahy and S. Louie, Phys. Rev. B **36** 3373 (1987).
[47] J. Kasper and S. Richards, Acta Cryst. **17** 752 (1964).
[48] S. Shcheka, M. Wiedenbeck, D. Frost, *et al.*, Earth Planet Sci. Lett. **245** 730 (2006).
[49] S. Ono, T. Kikegawa, Y. Ohishi, *et al.*, Am. Mineral. **90** 667 (2005).
[50] S. Ono, personal communication.
[51] D. Zahn and S. Leoni, Phys. Rev. Lett. **92** 250201 (2004).
[52] D. Zahn and S. Leoni, Z. Krist. **219** 345 (2004).
[53] C. Dellago, P. Bolhuis, F. Csajka, *et al.*, J. Chem. Phys. **108** 1964 (1998).
[54] S. Ono, T. Kikegawa and Y. Ohishi, J. Phys. Chem. Solids **65** 1527 (2004).
[55] S. Ono and Y. Ohishi, J. Phys. Chem. Solids **66** 1714 (2005).
[56] Oganov and Ono [26] found this structure by similarity with the structure of a high-pressure phase of Fe_2O_3 solved by S. Ono from powder diffraction in 2003 [54, 55]. For Fe_2O_3, the problem of cationic permutation does not exist.